Catalytic Hydrogenation of Post-Mature Hydrocarbon Source Rocks Under Deep-Derived Fluids: An Example of Early Cambrian Yurtus Formation, Tarim Basin, NW China

Huang Xiaowei[1,2], Jin Zhijun[2,3,4]*, Liu Quanyou[2,3]*, Meng Qingqiang[2,3], Zhu Dongya[2,3], Liu Jiayi[2,3] and Liu Jinzhong[5]

[1]School of Energy Resources, China University of Geosciences, Beijing, China, [2]State Key Laboratory of Shale Oil and Gas Enrichment Mechanisms and Effective Development, SINOPEC, Beijing, China, [3]Research Institute of Petroleum Exploration and Production, SINOPEC, Beijing, China, [4]Institute of Energy, Peking University, Beijing, China, [5]State Key Laboratory of Organic Geochemistry, Guangzhou Institute of Geochemistry, Chinese Academy of Sciences, Guangzhou, China

As a link between the internal and external basin, the deep derived fluids play a key role during the processes of hydrocarbon (HC) formation and accumulation in the form of organic-inorganic interaction. Two questions remain to be answered: How do deep-derived fluids affect HC generation in source rocks by carrying a large amount of matter and energy, especially in post-mature source rocks with weak HC generation capability? Can hydrogen and catalysts from deep sources significantly increase the HC generation potential of the source rock? In this study, we selected the post-mature kerogen samples of the early Cambrian Yurtus Formation in the Tarim Basin of China. Under the catalytic environment of $ZnCl_2$ and MoS_2, closed system gold tube thermal simulation experiments were conducted to quantitatively verify the contribution of catalytic hydrogenation to "HC promotion" by adding H_2. The catalytic hydrogenation increased the kerogen HC generation capacity by 1.4–2.1 times. The catalytic hydrogenation intensity reaction increased with temperature. The drying coefficient of the generated gas decreased significantly as the increasing yield of heavy HC gas. In the simulation experiment, alkane $\delta^{13}C$ becomes lighter after the catalytic hydrogenation experiment, while $\delta^{13}C_{CO2}$ becomes heavier. In the process of catalytic hydrogenation, the number of gaseous products catalyzed by $ZnCl_2$ is higher than that catalyzed by MoS_2 under the same conditions, indicating that $ZnCl_2$ is a better catalyst for the generation of gaseous yield. Meanwhile, Fischer-Tropsch synthesis (FFT) reaction was happened in the catalytic hydrogenation process. The simulation experiment demonstrates that hydrogen-rich components and metal elements in deep-derived fluids have significant catalytic hydrogenation effects on organic-rich matter, which improved the HC generation efficiency of post-mature source rocks.

Keywords: yurtus formation, simulation experiment, catalytic hydrogenation, gaseous yield, isotope fractionation

INTRODUCTION

The deep-derived fluids refer to the mantle source volatile fluid below the basement of the sedimentary basin, which is originated from the dehydrating fluid generated in the process of plate subduction or deep metamorphism, and the deep circulating fluid driven by the heat from the mantle or the deep shell source (Jin et al., 2002; Jin et al., 2004; Jin et al., 2007; Liu et al., 2018). A large amount of gas components carried by the deep-derived fluids contain volatile materials, such as H_2, CH_4, H_2S, CO_2, N_2, and He. As one of the main volatile fluids, the distribution of geologic H_2 (molecular hydrogen) is widespread in ocean ridges, active tectonic belts, and the Precambrian or Cenozoic strata distributed on land (Jeffrey and Kaplan, 1998; Allen and Seyfried, 2004; Newell et al., 2007; Tivey, 2007; Bradley and Summons, 2010; Sherwood-Lollar et al., 2014; Meng et al., 2015; Etiope, 2017; Guélard et al., 2017; Etiope and Whiticar, 2019; Bougault et al., 2019; Klein et al., 2019; Klein et al., 2020). H_2 has a variety of genetic types, including the release of deep magma degassing, the serpentinization of ultrabasic-basic rocks (Sherwood-Lollar et al., 2014; Etiope, 2017; Klein et al., 2019; Klein et al., 2020), radiolysis of water due to the presence of radioactive minerals (Sherwood-Lollar et al., 2014; Milesi et al., 2016), mechanical cracking of Si-bearing rock (Hirose et al., 2011; Telling et al., 2015), and the reduction of organic matter by microorganisms (Shuai, et al., 2010). The deep-derived fluids not only carry energy and hydrogen-rich matter, but a large amount of metal catalysts and other elements such as Mg, Fe, Mn, Ni, Zn, Mo, and Cu (Coveney, 1987; Pinto et al., 1999; Tivey, 2007; Proskurowski et al., 2008; Resing et al., 2015). Meanwhile, in sedimentary basins the enrichment of organic matter is normally accompanied by abundant metal elements (e.g., Fe, Mn, Zn, and Mo) (Lv et al., 2018).

The geological kerogen catalytic hydrogenation reaction is a reduction reaction that generates new products and is accompanied by energy conversion. To study the contribution of material conditions in organic-inorganic interactions to hydrocarbon (HC) generation from organic matter, previous studies examined different external hydrogen sources and catalysts (Hawkes, 1972; Jin et al., 2002; Jin et al, 2004). As the energy of the H-H bond is theoretically 436 kJ mol^{-1}, which is less than the H-OH bond energy of 497 kJ mol^{-1} (Luo, 2004), H_2 is easier to hydrogenate organic matter than H_2O under simulated experimental conditions (Jin et al., 2004). Lewan et al. (1979), Lewan, (1997)and Seewald (2003) confirmed that the contribution of exogenous H plays a key role in HC generation and distribution of underground HC components. Mango et al. (1996, 1997) showed in an open system that the reaction of exogenous hydrogen with organic matter promotes the rate of HC generation under the action of transition metals. Meng et al. (2015) confirmed that deep hydrogen-rich fluids can activate and increase the HC regeneration of ancient source rocks through experiments. Liu et al. (2016) showed that there is Fischer-Tropsch-type (FTT) interaction between H_2 and CO_2 produced by the thermal alteration of source rocks in the geological environment to synthesize HCs.

These deep-derived fluids can hydrogenate post-mature kerogen, thereby activating kerogen's ability to regenerate HCs, by activating the original inert carbon in kerogen and generating HCs (Meng et al., 2015). The post-mature kerogen is rich in polycyclic aromatic HC compounds and polymer groups and has a low H/C ratio. H is a hydrocarbon-generating restrictive reactant for high-maturity kerogen. The hydrocracking reaction can hydro-isomerize and crack (including ring-opening) aromatic compounds and macromolecular groups, i.e., break long-chain alkanes into short-chain alkanes, so that aromatic or naphthenic HCs can be opened to form long-chain alkanes. The hydrocracking reaction can further break the chain (Han, 2001) to promote the reactivation of kerogen to generate HCs (Liu et al., 2018; Liu et al., 2019). In order to simulate the geological regularities of catalytic hydrogenation more accurately in a more consistent environment with deep-derived fluids, on the basis of previous studies, we further optimized the hydrogen quantification in the simulation experiment. The main objectives of this work are to examine the potential of HC generation in high-maturity marine I-type kerogen in the quantitative hydrogenation process, which involves different catalysts under closed system conditions. Meanwhile, it provided to understand the characteristics of HC isotope fractionation of alkane gas under the influence of deep-derived fluids; and to provide theoretical support for the evaluation of organic HC generation.

EXPERIMENTAL SAMPLES AND METHODS

Experimental Samples

In this study, kerogen was selected from the argillaceous source rocks of the early Cambrian Yurtus Formation in the Dongergou section of the Tarim Basin. Kerogen (Ker) was type I with the vitrinite reflectance (Ro) of 1.91%. The experimental samples were approximately 200 meshes. Total organic carbon (TOC) content of kerogen is 64.0% with purification, atomic ratio H/C = 0.87, T_{max} = 530°C, pyrolysis parameter S_1 = 1.43 mg HC/g ker, S_2 = 10.95 mg HC/g ker, S_3 = 16.17 mg CO_2/g ker, hydrocarbon index (HI) = 18, oxygen index (OI) = 28. The catalysts used in this study, $ZnCl_2$ and MoS_2, had a particle size of 200 mesh and met the experimental analytical purity requirements. Deionized water was prepared in the laboratory, and H_2 was high-purity hydrogen gas containing 5% internal standard helium (He).

Experimental Method

The simulation experiment was conducted in the State Key Laboratory of Organic Geochemistry, Guangzhou Institute of Geochemistry, Chinese Academy of Sciences in a closed system composed of gold tubes. During the sample loading process, the loading method of solid-liquid samples described in detail by Liu and Tang (1998) was used. In short, we added the weighed kerogen powder, deionized water, and catalyst powder (10:10: 1, wt: wt: wt) into a gold tube (6 mm inner diameter and 70 mm length), which was welded and sealed for cleaning, placed the tube in an argon atmosphere for 25 min to replace the air in the tube, pinched the wall of the gold tube with manual pliers, and sealed the top port with argon arc welding to complete the loading steps. For the hydrogenation sample loading, we made sure precise

quantitative volume H_2 injected into a larger gold tube. The tube (10 mm inner diameter, 120 mm long) was used. The pre-solid and liquid reactant injection method was the same as above: when quantitatively injecting H_2 (containing 5% He as the internal standard gas), temperature control was carried out under room temperature (25°C) with two high-sensitivity pressure gauges connected in series to ensure the amount of H_2 injection using the principle of hydrogen gas replacement to effectively eliminate air interference. The mass of the reactants added to the tube was 40 mg kerogen powder, 40 mg deionized water, 4 mg catalyst powder, and 0.65 mg H_2. Then we pressed the top port of the gold tube with a pressure clamp to seal the hydrogen component inside the gold tube and flattened the port with the pressure clamp after the wall of the gold tube was welded by argon arc welding. Next, the gold tube was placed in hot water (>60°C) without bead-shaped bubbles overflowing to ensure gas tightness in the tube.

After the sample loading of gold tubes was completed, the tubes were placed in the high-temperature reaction kettle set for heating. The temperature was first raised in 2 h to reach each predetermined temperature point, and then constant heating was performed for 72 h. There were five groups of experimental samples with each set at six temperature points, 350°C, 375°C, 400°C, 450°C, 500°C, and 550°C. Group I is kerogen + deionized water, group II is kerogen + deionized water + $ZnCl_2$, group III is kerogen + deionized water + MoS_2, group IV is kerogen + deionized water + $ZnCl_2$+H_2, group V is kerogen + deionized water + MoS_2+H_2. The simulated experimental pressure was constant at 500 bar, and the abnormal pressure change in the kettle did not exceed 1 bar.

Experimental Analysis

Following the research method of Pan et al. (2006) and Jia et al. (2014), the gold tube was removed and carefully placed into a custom-made vacuum glass tube. The vacuum tube was connected to an Agilent 6890 N full-component gas chromatograph (GC), which was modified by Wasson ECE Instrumentation for determination of gas molecular composition. The GC contains three detection channels, one flame ionization detector (FID), and two thermal conductivity detectors (TCD). N_2 was the carrier gases for the organic detection channel (FID) and inorganic channel (TCD1), and He was the carrier gas for hydrogen and helium detection channel (TCD2). The detection column was a Paraplot Q-type capillary column. The vacuum environment of the system was maintained by connecting a vacuum pump in the glass tube and piercing the gold tube inside to release the gas component. There are two valves connected in series to the vacuum tube and the chromatograph, which are used to measure the pressure change of the gas component and release part of the gas into the chromatograph to measure its molecular composition. We determined the type and composition of the gas products through different detection response values and corresponding time points. The method used the peak areas of different detection values of FID and TCD to complete the quantification of different gaseous products generated by the peak area ratio of the known quantitative standard gas (Liu and Tang, 1998).

After the GC detection analysis, a gas-tight syringe was used to extract a small amount of gas was extracted from the vacuum tube using a compact gas sampling needle for the carbon and hydrogen isotope analysis. The ratios of carbon and hydrogen isotopes refer to the Vienna Peedee belemnite standard (VPDB). The carbon isotope ratio detection and analysis were performed using a GV Isoprime IRMS interfaced with an Agilent 6890 N-Isoprime 100 instrument. The detection value of each sample was measured two to three times. If there was no obvious difference between the previous two detection values, the average value was taken as the same position value of the sample. If the difference between the first two test values was large, the third test was required, and the average value of the two adjacent values in three tests was taken as the final sample isotope composition. The carbon isotope analysis accuracy of this equipment was within ±0.4‰. Hydrogen isotope ratio detection was performed using the Thermo Trace GC 1310-Delta V Advantage instrument. The detection method was consistent with the carbon isotope analysis, and the hydrogen isotope accuracy was within ±3‰. During the detection process, the pre-determined $\delta^{13}C$ value calibration gases were periodically analyzed to check the accuracy of the measured value.

RESULTS

Total Gas Yield

The total gas yield of different simulated experimental samples showed an upward trend with increasing temperature (**Table 1**). The total gas yield of group I was measured at the initial temperature of 350°C at 56.6 m^3/t Ker, and the yield increased substantially after 400°C. At the highest temperature of 550°C, the yield reached a maximum value of 241.8 m^3/t Ker. After the catalysts $ZnCl_2$ and MoS_2 were added to groups II and III, the total gas yield increased from the lowest values of 70.0 m^3/t Ker (350°C) and 70.5 m^3/t Ker (350°C), respectively, and began to increase significantly at 400°C. The maximum yields were 513.4 m^3/t Ker and 347.5 m^3/t Ker, which were 2.1 to 1.4 times the maximum value in group I, respectively. The addition of $ZnCl_2$ and MoS_2 significantly promoted the reaction, and the yield increased more by the addition of $ZnCl_2$ than MoS_2, and the gas increase was mainly from CH_4 and CO_2. In groups IV and V, the total gas yields (without accounting for H_2 yield) were 55.7 m^3/t Ker (350°C) and 29.2 m^3/t Ker (350°C), respectively, and then the yield increased greatly at 375°C. The maximum yields were 506.5 m^3/t Ker and 368.4 m^3/t Ker at 550°C, respectively. Compared with groups II and III, the groups IV and V showed little change in the total yield. With the addition of H_2 reaction resulted in the alkane yield increased, but the CO_2 yield decreased, resulting in an insignificant change in the total gas yield overall.

Product Components

In terms of the total yield distribution of gaseous HCs, the $\sum C_{1-5}$ yield of group I increased continuously with temperature, and the maximum yield was 99.49 m^3/t Ker. After the catalysts $ZnCl_2$ and MoS_2 were added to groups II and III, the maximum yields of $\sum C_{1-5}$ were 208.22 m^3/t Ker and 137.77 m^3/t Ker, which were

TABLE 1 | Types and concentrations (m³/t Ker) of gas generated during the catalytic pyrolysis experiments at 350°C/72 h, 375°C/72 h, 400°C/72 h, 450°C/72 h, 500°C/72 h, and 550°C/72 h.

Group	Temp (°C)	CO_2	CH_4	C_2H_6	C_3H_8	iC_4	nC_4	iC_5	nC_5	H_2
						Yield (m³/t ker)				
I	350	55.57	0.95	0.11	0.00	0.00	0.00	0.00	0.00	0.00
	375	57.97	2.78	0.21	0.00	0.00	0.00	0.00	0.00	0.00
	400	67.72	12.57	0.51	0.00	0.00	0.00	0.00	0.00	0.00
	450	76.45	29.20	0.67	0.00	0.00	0.00	0.00	0.00	0.00
	500	98.08	52.99	0.72	0.02	0.01	0.03	0.02	0.04	0.01
	550	142.25	98.55	0.80	0.07	0.05	0.03	0.00	0.00	0.02
II	350	69.00	0.83	0.10	0.01	0.00	0.00	0.00	0.00	0.03
	375	77.68	4.46	0.34	0.01	0.00	0.00	0.00	0.00	0.16
	400	80.58	12.11	0.68	0.02	0.00	0.00	0.00	0.00	0.45
	450	108.17	44.09	0.93	0.00	0.00	0.00	0.00	0.00	2.57
	500	160.11	99.93	1.16	0.03	0.00	0.00	0.00	0.00	9.03
	550	280.91	207.56	0.65	0.01	0.00	0.00	0.00	0.00	24.27
III	350	69.47	0.86	0.11	0.01	0.00	0.00	0.00	0.00	0.00
	375	79.05	4.23	0.29	0.01	0.00	0.00	0.00	0.00	0.00
	400	80.06	10.08	0.49	0.01	0.00	0.00	0.00	0.00	0.02
	450	91.92	38.31	0.61	0.01	0.00	0.00	0.00	0.00	0.84
	500	126.29	69.88	0.64	0.01	0.00	0.00	0.00	0.00	4.61
	550	192.35	136.89	0.85	0.01	0.00	0.00	0.00	0.00	17.43
IV	350	35.70	11.07	3.20	2.97	0.39	1.62	0.52	0.23	-
	375	38.64	18.09	5.35	5.09	0.73	2.94	0.85	0.38	-
	400	39.60	41.31	14.44	16.91	2.44	7.90	1.79	0.79	-
	450	41.01	117.10	42.49	34.35	4.77	4.57	0.54	0.09	-
	500	54.54	225.51	64.76	0.94	0.02	0.05	0.01	0.00	-
	550	109.11	369.82	5.06	0.04	0.19	0.21	0.00	0.00	-
V	350	15.66	10.55	1.53	0.82	0.08	0.41	0.11	0.08	-
	375	20.92	14.33	3.77	3.45	0.35	1.90	0.50	0.57	-
	400	27.75	31.86	10.57	11.81	1.30	5.99	1.28	0.98	-
	450	29.79	87.35	30.90	21.84	2.19	2.10	0.10	0.13	-
	500	41.24	164.67	42.59	0.44	0.01	0.03	0.01	0.08	-
	550	76.06	283.63	8.61	0.04	0.00	0.00	0.00	0.03	-

increased 2.1 and 1.4 times as much as group I, respectively. It proved that the addition of $ZnCl_2$ and MoS_2 significantly promoted the generation of the gas components. In groups IV and V, the maximum yields of $\sum C_{1-5}$ were 375.34 m^3/t Ker and 292.32 m^3/t Ker, representing 1.8 and 2.1 times increase compared to groups II and III. The catalytic hydrogenation.

The methane (C_1) yield increased with temperature and reached the maximum at 550°C. The maximum C_1 yield in group I was 98.55 m^3/t Ker. When the catalysts $ZnCl_2$ and MoS_2 were added to groups II and III, the maximum yields of C_1 were 207.56 m^3/t Ker and 136.89 m^3/t Ker, which were 2.0 and 1.4 times as much as the yield of group I, respectively. In groups IV and V, the maximum yields of C_1 were 369.82 m^3/t Ker and 283.63 m^3/t Ker, respectively, which were 1.8 and 2.1 times the yields of groups II and III (**Figure 1**).

The change in the ethane (C_2) yield of group I with temperature was very small, and the maximum C_2 yield was 0.8 m^3/t Ker (500°C). After the catalysts $ZnCl_2$ and MoS_2 were added to groups II and III, the maximum C_2 yields were 1.16 m^3/t Ker and 0.85 m^3/t Ker, respectively. The addition of $ZnCl_2$ and MoS_2 did not increase the C_2 yield significantly. In groups IV and V, the maximum yields of C_2 were 64.76 m^3/t Ker and 42.59 m^3/t Ker (both 500°C), which were 80 and 50 times those of groups II and III without H_2, respectively. Exogenous H_2 reacts more easily than H_2O to promote the generation of C_2 (**Figure 2**).

The change in the propane (C_3) yield of group I with temperature was close to 0.0 m^3/t Ker. After adding the catalysts $ZnCl_2$ and MoS_2 to groups II and III, the change in the C_3 yield was still 0.0 m^3/t Ker, indicating that the addition of metal salts did not significantly increase the C_3 yield. In groups IV and V, the maximum yields of C_3 were 34.4 m^3/t Ker and 21.8 m^3/t Ker (450°C), respectively; the addition of external H_2 and catalysts exceedingly improved the C_3 yield (**Figure 3**). The comparison of the results of C_1, C_2, and C_3 shows that the addition of exogenous H_2 increases the HC generation yield, and the peak temperature of HC generation decreases sequentially with the increasing carbon number.

The catalytic addition of the H cracking reaction had a significant effect on the drying coefficient of natural gas (C_1/$\sum C_{1-5}$) (**Table 1**). The C_1/$\sum C_{1-5}$ ratio of group I (kerogen + deionized water) increased with temperature, from a minimum of 0.90 (350°C) to 0.99 (550°C). When the catalysts $ZnCl_2$ and MoS_2 were added to groups II and III, the C_1/$\sum C_{1-5}$ ratio became larger with increasing temperature at the ratios of 0.89–1.00 and 0.87–0.99, respectively. The addition of $ZnCl_2$ and MoS_2 promoted the formation of C_{2+} HCs at relatively low temperatures (≤400°C). After adding H_2 and catalysts $ZnCl_2$ and MoS_2, the addition of exogenous H_2 greatly increased the heavy HC (C_{2+}) components, and the C_1/$\sum C_{1-5}$ ratios at 350°C were 0.55 and 0.78, respectively. The C_1/$\sum C_{1-5}$ ratio gradually decreased with the increasing temperature and dropped to the lowest point at 0.48 and 0.50, respectively, at 400°C. After 400°C, C_1 produced by the hydrocracking of kerogen continued to increase, as well as C_{2+} HCs in the product. The conversion to C_1 significantly increased the C_1 yield, and the natural gas drying coefficient reached the maximum values of 0.99 and 0.97 at 550°C.
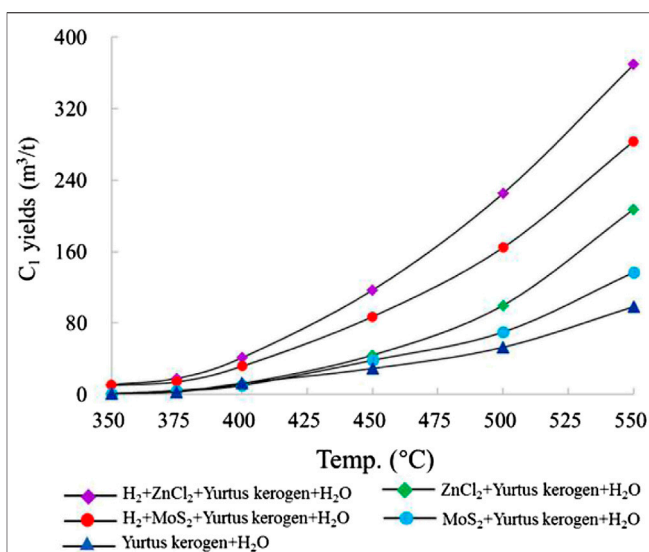

FIGURE 1 | Characteristics of C_1 yield simulated under different catalytic hydrogenation control conditions of the closed system.
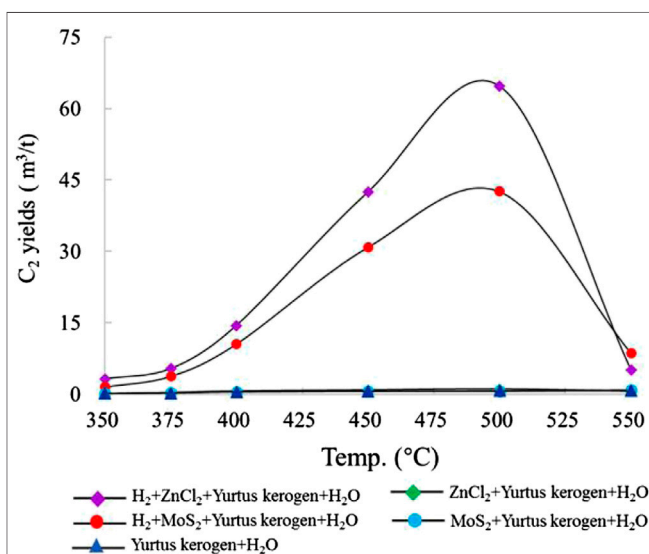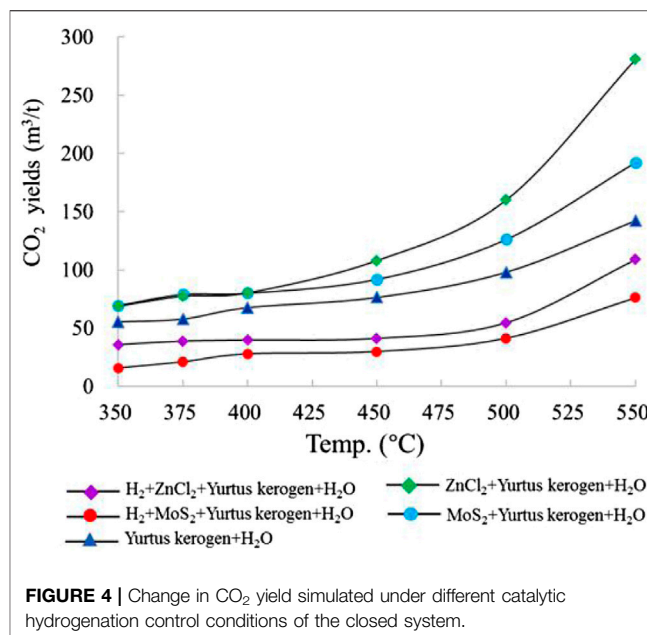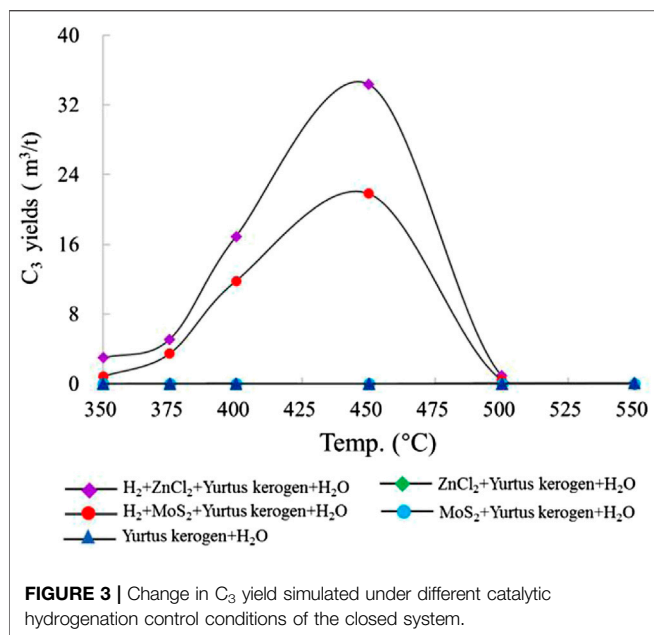

FIGURE 2 | Change in C_2 yield simulated under different catalytic hydrogenation control conditions of the closed system.

The CO_2 yield in each group of experiments increased with increasing temperature and reached the maximum value at 550°C. The CO_2 yield of group I gradually increased with increasing temperature, and the maximum CO_2 yield was 142.25 m^3/t Ker. In groups II and III, with the addition of catalysts $ZnCl_2$ and MoS_2, the maximum yields of CO_2 were 280.91 m^3/t Ker and 192.35 m^3/t Ker, respectively, which are 2.0 and 1.4 times the maximum yield without the addition of the catalysts. The increase in CO_2 and HC components was similar, indicating that the metal ions mainly catalyze the lysis of kerogen itself rather than decomposing the bond between H and O. The CO_2 yields in

FIGURE 3 | Change in C_3 yield simulated under different catalytic hydrogenation control conditions of the closed system.

FIGURE 4 | Change in CO_2 yield simulated under different catalytic hydrogenation control conditions of the closed system.

groups IV and V were 0.39–0.40 times those of groups II and III, respectively (**Figure 4**). The significant decrease in the yield of CO_2 resulted from the reaction that occurred with the addition of H_2.

The experimental comparison of groups I, II, and III showed that the H_2 yield did not increase significantly with temperature (the highest is 0.02 m^3/t Ker at 550°C in group I), but the maximum yields after adding $ZnCl_2$ and MoS_2 were 24.27 m^3/t Ker and 17.43 m^3/t Ker at 550°C. The yield increased by one to two orders of magnitude, indicating that the H_2 production was significantly promoted by the addition of catalysts, combined with the C_2 yield. The dominant reason of the H increase is the cracking of organic matter.

Product Component Carbon Isotope Changes

The results show that $\delta^{13}C$ becomes heavier with increasing temperature. Since kerogen of the Yurtus Formation is at a high maturity stage, only C_1, C_2, and CO_2 isotope values can be effectively detected in product components. For the $\delta^{13}C$ value of gaseous HCs under different control conditions at the same temperature point, the $\delta^{13}C$ value of each gaseous HCs increased with the intensity of reaction between catalysis and hydrogen addition (**Table 2**). The $\delta^{13}C_1$ value of group I increased continuously with the increase in temperature from −39.8 to −34.9‰. When $ZnCl_2$ and MoS_2 were added to groups II and III, the $\delta^{13}C_1$ values changed from −44.7 to −36.7‰ and from −43.6 to −36.2‰. In groups IV and V, the $\delta^{13}C_1$ values changed from −45.9 to −40.2‰ and from −52.4 to −43.4‰, showing an increase before the 400°C stage, then a decrease in the 400–450°C interval, and finally becoming heavier with increasing temperature. For the C_1 yield after 400°C, catalytic hydrocracking plays a major role in promoting the disproportionation of small low-carbon

molecules. Since the bond energy of ^{12}C–^{12}C is less than the bond energy of ^{12}C–^{13}C, the $\delta^{13}C_1$ fractionation follows; as the intensity of catalytic hydrogenation increases, $\delta^{13}C_1$ becomes lighter (**Figure 5**).

The $\delta^{13}C_2$ value increased sequentially with the increasing temperature. In group I, the value of $\delta^{13}C_2$ changed from −28.2 to −24.4‰ at 350–400°C. After 400°C, the $\delta^{13}C_2$ value only changed from −24.4 to −23.6‰. In groups II and III with catalysts $ZnCl_2$ and MoS_2, the $\delta^{13}C_2$ value was generally stable, similar to group I, changing from −29.9 to −24.0‰ and from −29.1 to −23.7‰, respectively. The addition of $ZnCl_2$ and MoS_2 promoted the reaction and the exchange of C elements to a lesser extent. The $\delta^{13}C_2$ value changed in groups IV and V from −38.4 to −14.1‰ and from −37.6 to −12.1‰, indicating that catalytic hydrogenation significantly increases the formation of C_2 and the exchange of C elements. At 550°C, the $\delta^{13}C_2$ value was the largest because the addition of H_2 promoted the catalytic cracking reaction. When the temperature exceeded the gas generation window (<500°C), a large amount of C_2 cracked to form C_1, resulting in an abnormally large $\delta^{13}C_2$ value (**Figure 6**).

As one of the main reaction products, the CO_2 isotope fractionation value is mainly controlled by its own molecular quality. The comparison of the experimental results between the hydrogenated and unhydrogenated groups showed that the $\delta^{13}C_{CO2}$ value in the hydrogenated group was larger than the unhydrogenated group, which is negatively correlated with the change in the fractional distillation of the $\delta^{13}C$ value of alkanes. The $\delta^{13}C_{CO2}$ value of CO_2 generated by hydrocracking was relatively stable. The $\delta^{13}C_{CO2}$ values of groups I, II, and III were distributed between −35‰ and −33‰. The $\delta^{13}C_{CO2}$ values in groups IV and V showed a decreasing trend first and then an increasing trend. The participation of $ZnCl_2$ catalyst increased the $\delta^{13}C_{CO2}$ value of the product. The joint addition of H_2 and the catalyst further increased the fractionation of the $\delta^{13}C_{CO2}$ value.

TABLE 2 | δ^{13}C values of gas generated during the catalytic pyrolysis experiments at 350°C/72 h, 375°C/72 h, 400°C/72 h, 450°C/72 h, 500°C/72 h, and 550°C/72 h.

Group	Temp. (°C)	$\delta^{13}C_{CO2}$	$\delta^{13}C_1$ ‰ (VPDB)	$\delta^{13}C_2$
I	350	−34.6	-39.8	−28.2
	375	−34.0	−39.4	−27.3
	400	−33.8	−38.0	−24.4
	450	−33.9	−35.7	−24.3
	500	−34.1	−35.2	−24.9
	550	−34.7	−34.9	−23.6
II	350	−34.0	−44.7	−29.9
	375	−33.9	−42.9	−27.5
	400	−33.7	−42.7	−27.0
	450	−33.2	−40.0	−25.0
	500	−33.4	−37.0	−24.9
	550	−33.5	−36.7	−24.0
III	350	−34.5	−43.6	−29.1
	375	−33.4	−41.6	−27.5
	400	−33.8	−40.8	−25.6
	450	−33.6	−37.4	−25.6
	500	−33.7	−36.2	−25.3
	550	-34.9	−36.2	−23.7
IV	350	−32.7	−45.9	−38.4
	375	−33.1	−45.0	−38.6
	400	−33.3	−43.7	−39.4
	450	−33.4	−44.1	−37.4
	500	−32.4	−43.1	−29.5
	550	−32.1	−40.2	−14.1
V	350	−23.0	−52.4	−37.6
	375	−32.2	−45.4	−38.2
	400	−33.5	−43.9	−39.4
	450	−34.2	−44.6	−36.9
	500	−33.4	−44.0	−28.1
	550	−34.2	−43.4	−12.1

FIGURE 6 | Change in $\delta^{13}C_2$ simulated under different catalytic hydrogenation control conditions of the closed system.

FIGURE 7 | Change in $\delta^{13}CO_2$ simulated under different catalytic hydrogenation control conditions of the closed system.
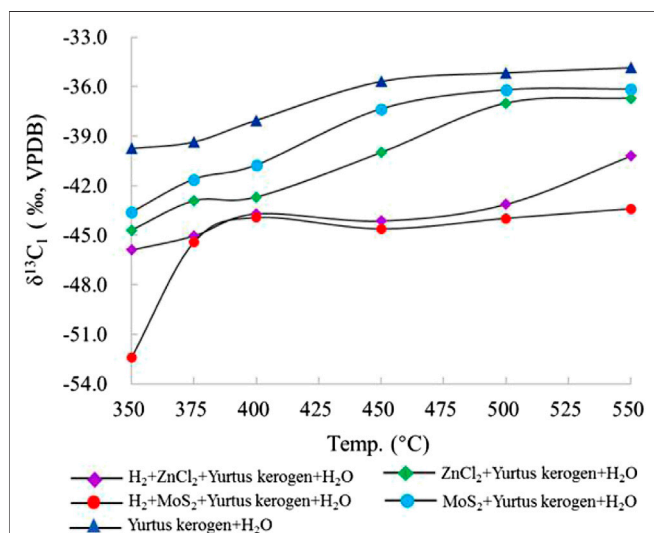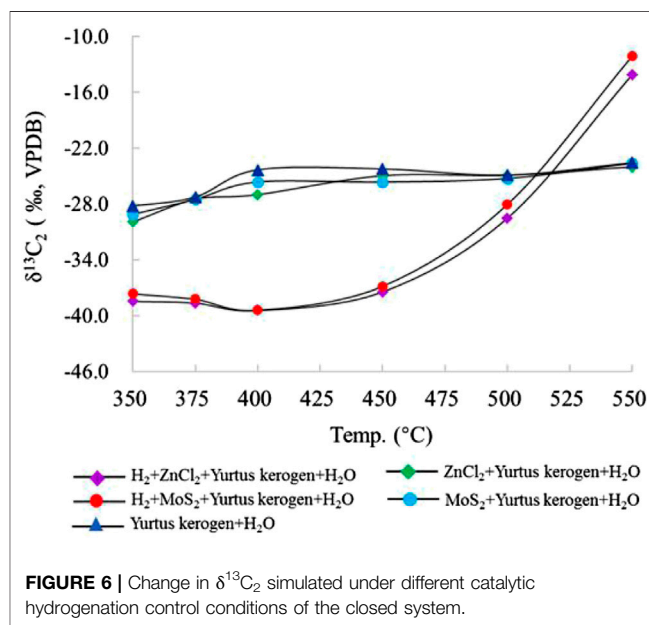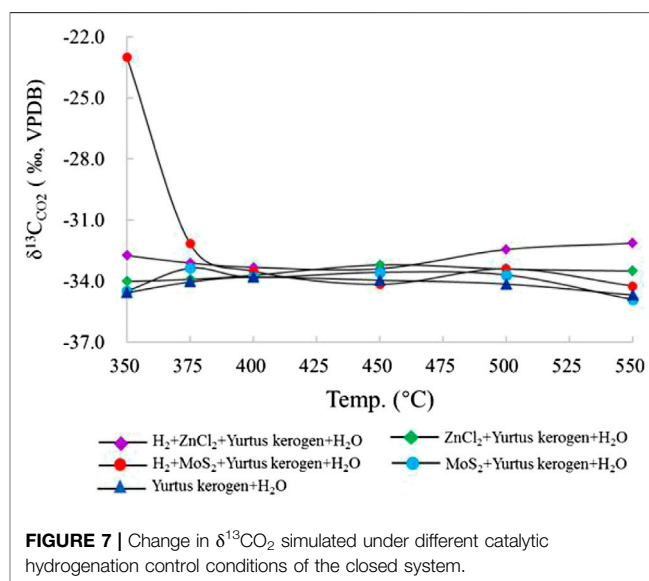

FIGURE 5 | Change in $\delta^{13}C_1$ simulated under different catalytic hydrogenation control conditions of the closed system.

The effect of MoS_2 on the $\delta^{13}C_{CO2}$ value was larger at the early stage of the reaction (**Figure 7**). At the same time, relative to the changes in δ^{13}C values for C_1 and C_2, the range of carbon isotope fractionation of CO_2 was smaller than that of alkanes because of the oxidative decarboxylation of its controlled long-chain HCs, rather than the bond energy difference controlled by the C-C bond leading to preferential cracking (Lu et al., 2010).

DISCUSSION

Catalytic Hydrogenation Mechanism

Catalytic hydrogenation showed that the yield and isotopic value of the gaseous product components changed significantly and were also accompanied by FTT synthesis reaction products. The source supply angle mainly depends on the control influence of H_2 and different metal elements in the reaction environment.

Product Component Comparison

The post-mature kerogen of the Yurtus Formation has very weak pyrolysis and HC generation capacity. With the increase in temperature and the catalysis of hydrogenation by different catalysts, the kerogen HC generation capacity significantly improved. As the most stable HC molecule, C_1 had an increased yield. In addition to the catalytic hydrogenation reaction of kerogen, there were other gaseous HCs produced by catalytic hydrocracking. The yield of different catalysts changed significantly. Under the same hydrogenation conditions, the yield of C_1 under the action of $ZnCl_2$ was greater than that of MoS_2, with a yield ratio of 1.0–1.4 and average of 1.3. The results of the control experiment between the experimental group with added H_2 and catalyst and the experimental group with catalyst only showed that the addition of H_2 delayed the decomposition of heavy HCs such as C_2 and C_3, leading to a higher temperature of HC generation peaks. Meanwhile, the heavy HC group bond energy was smaller than the methyl group energy, which led to the preferential participation of heavy HC groups in hydrocracking and thus to a significant increase in the yield of C_{2+} HCs and a significant reduction in the drying coefficient of the product. The addition of exogenous H_2 greatly changed the kerogen's own cracking mode, and heavy HC component C_{2+} increased significantly. It was well consistent with the results that the drying coefficient of the product gases with the increased intensity of catalytic hydrogenation is significantly lower than that of the ordinary geological environment (Lewan et al., 1979; Mango et al, 1994; Ma et al., 2018).

Change in the i/n-Alkane Ratio

Among gaseous HC components, normal paraffins are formed by free radical reactions, and isoparaffins are derived from free radical cracking on kerogen and asphalt branches under acidic cationic ion reaction (Eisma and Jurg, 1969; Almon and Johns, 1977; Kissin, 1987; Pan et al., 2006). The Yurtus Formation kerogen is high maturity, and the branched chains of its molecular structure is not developed; thus, the main source of isoparaffin is the acidification cation reaction. Thompson and Creath, (1966) showed that in North American industrial HC reservoirs mainly generated by free radical HC generation, the iC_4/nC_4 ratio is around 0.5, generally not greater than 1.0; the iC_5/nC_5 ratio is around 1.0 and generally less than 2.0. In this study, the comparison of the same component at the same temperature showed that the value of iC_n/nC_n under the action of $ZnCl_2$ was larger than MoS_2. For the products of butane (C_4), from the initial temperature of 350°C–400°C, the iC_4/nC_4 value of the products produced by the two catalysts was relatively stable, ranging from 0.241 to 0.309 and 0.184 to 0.217, respectively. The maximum values were 1.045 and 1.042, respectively, at 450°C. For the products of pentane (C_5), the temperature changed greatly from the initial temperature of 350°C–500°C; the range of the iC_5/nC_5 ratio under the action of $ZnCl_2$ was 2.200–6.252 and under the action of MoS_2 was 0.096–1.409 (Table 1, Figure 8). The results showed that under the action of $ZnCl_2$, more HCs were generated by the cationic reaction, which promoted more formation of the isoparaffins. The higher the temperature is, the more significant changes in the cationic reaction are. The results further reveal that the catalytic effect of $ZnCl_2$ on promoting HC generation by cation reaction is stronger than that of MoS_2.

Reaction Mechanism

HC generation of catalytic hydrogenation is mainly carried out in the form of H radicals and H ions. There are two modes of catalysis: "Lewis acid" catalysis and "Brønsted acid" catalytic processes (Figure 9). When performing Lewis acid site catalytic processes, the main chemical reactions are decarboxylation and C-C bond breaking (Li et al., 2002; He et al., 2011; Ma et al., 2018). Since the Lewis acid site composed of Zn^{2+} or Mo^{2+} is an empty orbital position with high affinity for electrons, when the organic matter is decarboxylated, Zn^{2+} or Mo^{2+} at this position gets an electron from the adsorbed organic molecule, and carboxylic acid loses CO_2. Free radicals further undergo a rearrangement reaction with H radicals, leading to the breakage of the C-C bond and the formation of free HCs with shorter bond lengths. The product of the decarboxylation reaction is mainly CO_2. The breakage of the C-C bond mainly promotes the generation of free HCs. When performing Brønsted acid catalytic processes, through contact with Zn^{2+} and Mo^{2+}, H_2 or water molecule lose an electron to generate H ions, promoting the kerogen unsaturated cycloalkane addition reaction. As the hydrogenation reaction continues, low-molecular-weight saturated chain HCs are eventually formed (Wu et al., 2012; Ma et al., 2018).
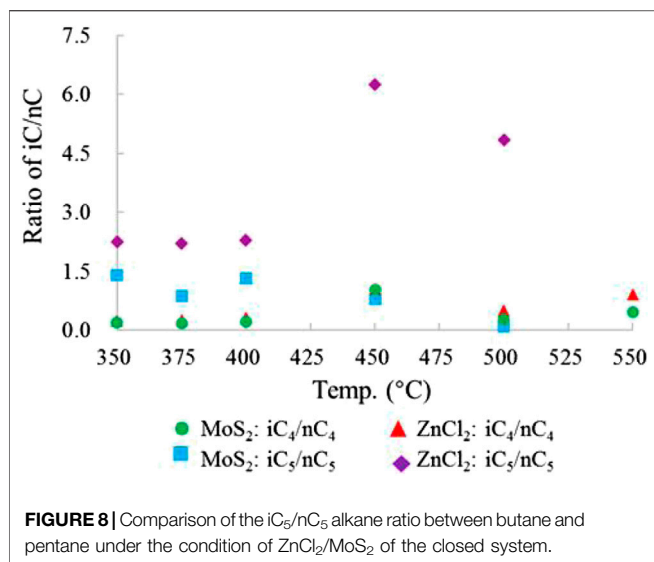
The yield results show that Zn^{2+} has a better catalytic effect than Mo^{2+} because Zn^{2+} has a more stable and long-lasting catalytic activity than Mo^{2+}, and it is easier to fully contact the reactants. The chemical properties of Cl^- are extremely stable. Previous studies suggest that Cl^- has a certain inhibitory effect on the catalyzed cracking of kerogen (Li et al., 2002). In the catalytic hydrogenation experiment of H_2, $ZnCl_2$ shows a strong catalytic effect on hydrogen generation. S^{2-} reacts with H_2 to generate part of H_2S, which has a catalytic effect on HC generation (He et al., 2011), but the product test results show that the H_2S content is relatively low, and the catalytic contribution is not significant.

Stable Carbon and Hydrogen Isotope Change Mechanism

$\delta^{13}C_1/\delta^{13}C_2$

For the HC isotope composition of oil and natural gas, relative to its parent material, kerogen is lean in ^{13}C and ^2H. This is because the kerogen ^{12}C–^{12}C bond and the C-C bond in ^1H-CC-^1H are more easily broken than the ^{12}C–^{13}C bond and the ^2H-CC-^1H CC bond, thereby allowing lighter isotopes to enter HC (Lu et al., 2010).

The change in $\delta^{13}C_1$-$\delta^{13}C_2$ values can reflect the catalytic hydrogenation effects effectively. The data of groups I, II and III showed that $\delta^{13}C_1$-$\delta^{13}C_2$ has a strong linear relationship (Figure 10). After adding the catalysts, the change in the $\delta^{13}C_1$-$\delta^{13}C_2$ value was decreased significantly and the range changed widely, but C_2 yield changed little (Figure 2). The results showed that C_2 mainly promotes the elemental exchange between carbon isotopes after the catalyst were added and has little effect on the yield reaction equilibrium. The comparison of the experimental results showed that the catalyst addition leads to lighter $\delta^{13}C_1$ and $\delta^{13}C_2$. Meanwhile, the

FIGURE 8 | Comparison of the iC_5/nC_5 alkane ratio between butane and pentane under the condition of $ZnCl_2/MoS_2$ of the closed system.
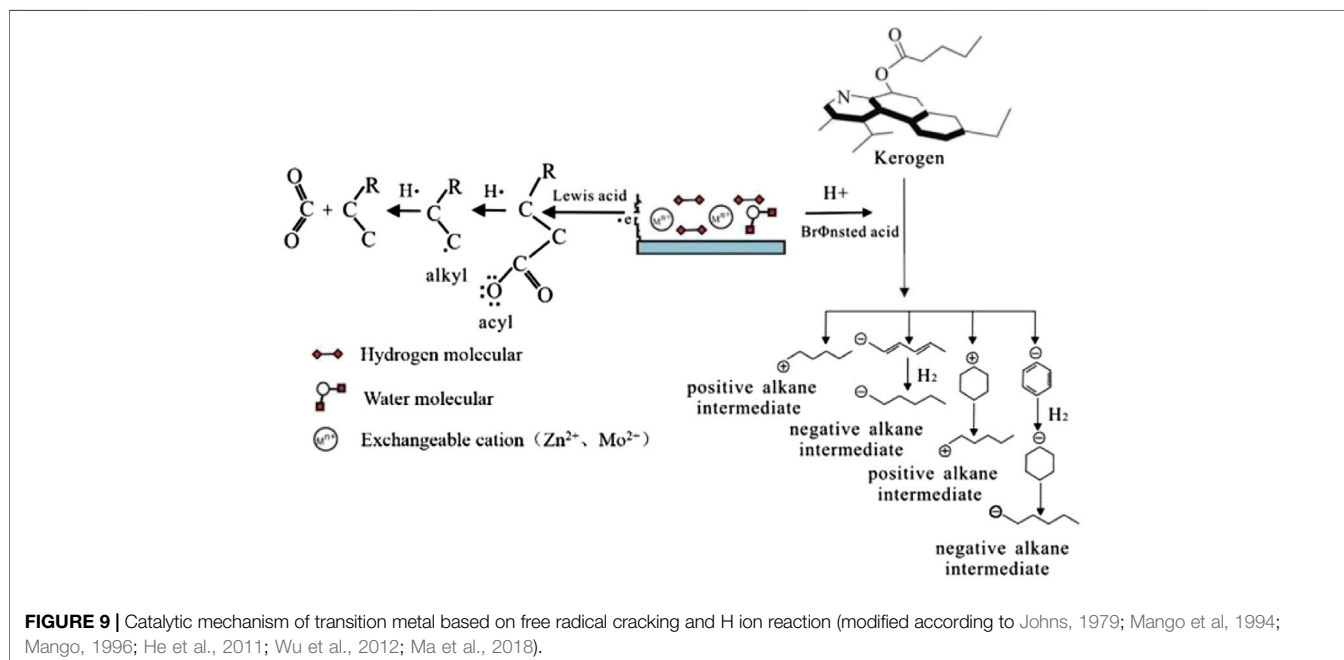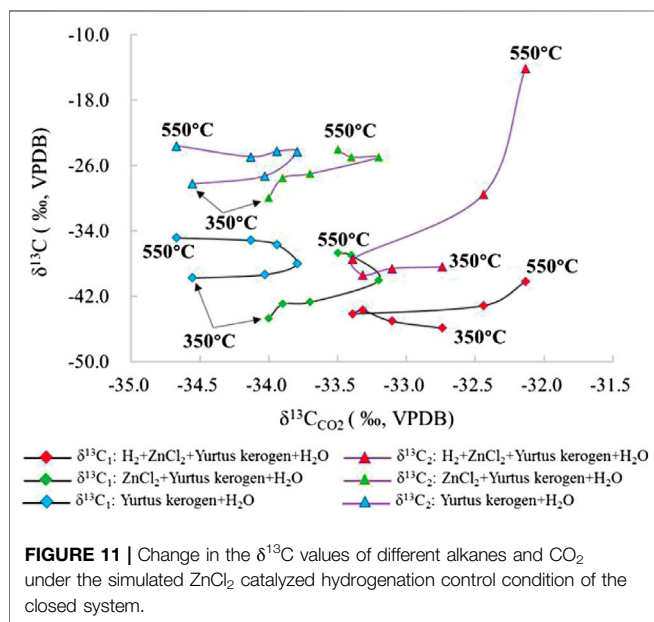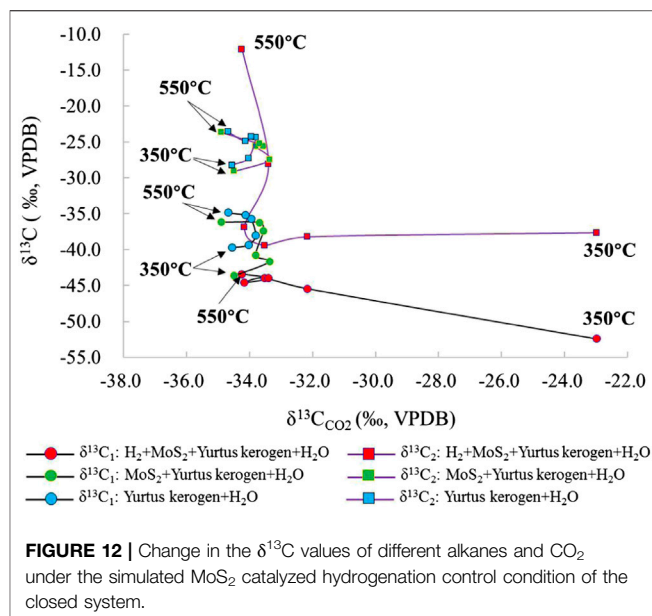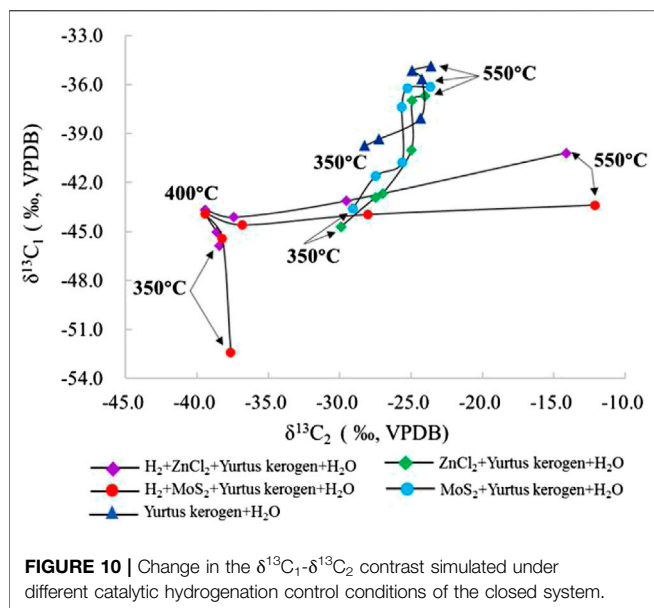
metal ions are involved in enhancing the reaction process and promoting the isotope fractionation level during the reaction. The catalytic hydrogenation extremely promotes the activation of the carbon source in post-mature kerogen. Within a certain temperature range (≤450°C), the distribution of $\delta^{13}C_1$-$\delta^{13}C_2$ is clustered and distributed in a stable lighter interval. At 500°C, the $\delta^{13}C_1/\delta^{13}C_2$ ratio is close to the range with no H_2 added. The C_2 component passed the peak of HC generation because the C_2 component with a smaller $\delta^{13}C$ value starts to crack into C_1, which led to the leaving C_2 with heavier $\delta^{13}C$. At the same time, C_3 cracked completely due to the $\delta^{13}C$ kinetic fractionation to promote the formation of lighter $\delta^{13}C_1$ and heavier $\delta^{13}C_2$.

Restricted by high temperature and the amount of carbon material, the heavier carbon content retained in generated C_2 increases at 550°C, resulting in larger change of linear variations. It also implies the $\delta^{13}C_1$-$\delta^{13}C_2$ parameters can provide supplementary verification to evaluate whether the HC generation process of source rocks was affected by catalytic hydrogenation in sedimentary basins.

Relationship Between CO_2 and Alkane $\delta^{13}C$

CO_2 is one of the main by-products of the reaction process. Its $\delta^{13}C$ fractionation change is opposite to that of alkane $\delta^{13}C$. $\delta^{13}C_{CO2}$ increases with the enhancing intensity in the reaction (**Figures 11**, **12**). When the catalytic hydrogenation stage is weak, the kerogen HC generation is mainly carried out by self-cracking; thus, the changes in kerogen $\delta^{13}C$ in the low temperature stage are greatly affected by temperature and the external H_2 participation in the reaction. The $\delta^{13}C_{CO2}$ value became larger accompanied by an increasing intensity of the catalytic reaction. In group I, the $\delta^{13}C_{CO2}$ change from the large to the small was at the 400 °C inflection point. In group II and III, the $\delta^{13}C_{CO2}$ change from large to small was at the 450°C inflection point and the HC generation mode of kerogen was affected distinctly by the catalytic elements during pyrolysis reaction. In group IV and V, the addition of H_2 changed the characteristics of the original kerogen evolution process and promoted isotope exchange in the HC generation. The change in $\delta^{13}C_{CO2}$ from lighter to heavier was mainly controlled by the dynamic fractionation of carbon isotope of CO_2. The maximum $\delta^{13}C_{CO2}$ temperature under the action of $ZnCl_2$ is delayed compared to that under the action of MoS_2. The $\delta^{13}C_2$ value under the action of $ZnCl_2$ is less than that under the action of MoS_2, which demonstrates that the catalytic effect of $ZnCl_2$ under the same conditions is stronger than that of MoS_2.

FIGURE 9 | Catalytic mechanism of transition metal based on free radical cracking and H ion reaction (modified according to Johns, 1979; Mango et al, 1994; Mango, 1996; He et al., 2011; Wu et al., 2012; Ma et al., 2018).

FIGURE 10 | Change in the $\delta^{13}C_1$-$\delta^{13}C_2$ contrast simulated under different catalytic hydrogenation control conditions of the closed system.

FIGURE 12 | Change in the $\delta^{13}C$ values of different alkanes and CO_2 under the simulated MoS_2 catalyzed hydrogenation control condition of the closed system.

FIGURE 11 | Change in the $\delta^{13}C$ values of different alkanes and CO_2 under the simulated $ZnCl_2$ catalyzed hydrogenation control condition of the closed system.

Accompanying Secondary Reaction—Fischer-Tropsch-Type Synthesis

As one of the main modes of inorganic HC generation, FTT synthesis is well verified in geological discoveries and experiments (Fu et al., 2007; Hosgörmez, 2007; McCollom, 2013; Suda et al., 2014; McCollom, 2016; Etiope, 2017; Liu et al., 2018) and greatly affected by the redox conditions of the environment. The catalytic hydrogenation experiment provides a good reduction environment and source supply conditions. As shown in **Figure 13**, the relationship between CO_2 and CH_4 in the catalytic hydrogenation state of $ZnCl_2$ was y = 1.1359x-17.687, R^2 = 0.9375. Under the catalytic hydrogenation state of MoS_2, the relationship

between CO_2 and CH_4 changed to y = 2.1496x-97.873, R^2 = 0.9533. Under the stable reaction at >400°C, the relationship between CO_2 and CH_4 changed to y = 1.9199x-73.472, R^2 = 0.9921, indicating that the decrease in the yield of CO_2 in the hydrogenation reaction showed a strong linear relationship with the increase in C_1. The CO_2 yield decreased rapidly at 375 °C owing to the solubility of water at high temperatures. In the high-temperature stage (≥400°C) under the catalytic state, the activation reaction of hydrogen radicals and carbon molecules was accelerated. In the catalytic hydrogenation reaction of CO_2, a large quantity of HCs and water mainly composed of C_1 are produced in the FTT synthesis reaction accompanying H_2 and CO_2. The change in the slope of the equation shows that the catalytic effect of $ZnCl_2$ on kerogen pyrolysis and HC generation is stronger than that of MoS_2.

With H_2 added to the HC generation reaction, the CO_2 yield decreased significantly. However, the CO_2 yield remained stable after falling to a certain value. The yield was stable under the influence of different temperature points. According to the $\delta^{13}C_{CO2}$ isotope change, a heavier trend in both H_2 added groups implies that ^{12}C is more likely to participate in the catalytic hydrogenation response than ^{13}C. Combined with the experimental results described in **Table 1**, **Figures 4, 13**, the addition of H_2 inhibited the CO_2 generation. The FTT synthesis decreased the generated CO_2 and H_2 yield. The results of the control experiment showed that the final CO_2 conversion rate was a constant under a different reaction environment. The amount of activated C with the H_2 addition reaction indicated that activated C reactants would not react in the geological environment.

The catalysis reaction by the addition of H_2 was carried out in a neutral reduction system, and the FTT synthesis accompanied by CO_2 generated HCs, which had a significant effect on the total HC yield. In geological processes, the FTT synthesis reaction plays an important role as a link between the deep hydrogen-rich fluid and the hydrogen generation of post-mature organic matter.
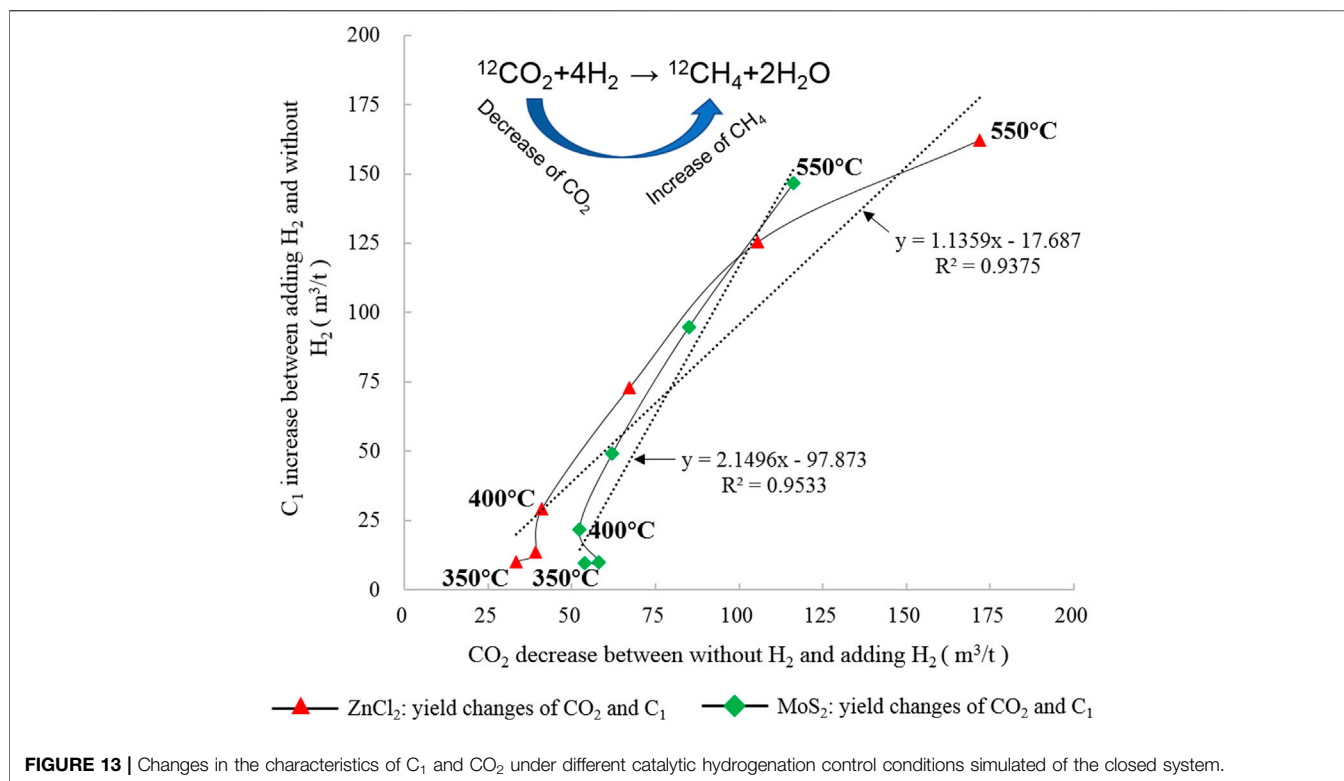
FIGURE 13 | Changes in the characteristics of C_1 and CO_2 under different catalytic hydrogenation control conditions simulated of the closed system.

CONCLUSION

For the ancient source rocks of the Yurtus Formation in the Tarim Basin, the catalytic substances and exogenous hydrogen carried under deep-derived fluids can "secondarily generate HCs" for the activation of source rocks. $ZnCl_2$ and MoS_2 have a strong catalytic effect on the reaction of post-mature kerogen and H_2. Catalytic addition of H_2 promotes the HC generation capacity of kerogen and the increase in HCs by 0.4–1.1 times, significantly reduces the natural gas drying coefficient, and promotes FTT synthesis of secondary reactions. Isotope fractionation mainly follows the laws of kinetics and shows good identification characteristics. By comparing the composition of gaseous products and isotope characteristics, the catalytic effect of $ZnCl_2$ is stronger than MoS_2 under the same conditions. Meanwhile, it implies deep-derived hydrogen fluids containing Zn, Mo and other metal elements can make a remarkable contribution to reactivate the post-mature source rocks for HC generation.

DATA AVAILABILITY STATEMENT

The original contributions presented in the study are included in the article/Supplementary Material, further inquiries can be directed to the corresponding authors.

REFERENCES

Allen, D. E., and Seyfried, W. E., Jr. (2004). Serpentinization and heat generation: constraints from Lost City and Rainbow hydrothermal systems 1 1Associate editor: J. C. Alt. *Geochem. Cosmochim. Acta.* 68 (6), 1347–1354. doi:10.1016/j.gca.2003.09.003

AUTHOR CONTRIBUTIONS

FUNDING

ACKNOWLEDGMENTS

Almon, W. R., and Johns, W. D. (1977). "Petroleum-forming reactions. The mechanism and rate of clay catalyzed fatty acid decarboxylation," in *Advances in organic Geochemistry* Editors R. Campos and J. Goni (Madrid: Enadimsa), 157–172.

Bougault, H., and Dpt, M.G. (2019). Hydrothermal hydrogen and methane: scientific insight a new potential resource? [J]. Mines & carrieres. *Les techniques, 196(hors series),* 73–80.

Bradley, A. S., and Summons, R. E. (2010). Multiple origins of methane at the lost city hydrothermal field. *Earth Planet. Sci. Lett.* 297 (1–2), 34–41. doi:10.1016/j.epsl.2010.05.034

Coveney, R.M.J. (1987). Serpentinization and the origin of hydrogen gas in Kansas[J]. *American Association of Petroleum Geologists Bulletin,* 71 (1), 39–48.

Eisma, E., and Jurg, J. W. (1969). "Fundamental aspects of the generation of petroleum," in *Organic Geochemistry, methods and results*. Editors G. Eglinton and M.T.J. Murphy (Berlin: Springer-Verlag), 675–698.

Etiope, G. (2017). Abiotic methane in continental serpentinization sites: an overview. *Procedia Earth Planet. Sci.* 17, 9–12. doi:10.1016/j.proeps.2016.12.006

Etiope, G., and Whiticar, M. J. (2019). Abiotic methane in continental ultramafic rock systems: towards a genetic model. *Appl. Geochem.* 102, 139–152. doi:10.1016/j.apgeochem.2019.01.012

Fu, Q., Sherwood Lollar, B., Horita, J., Lacrampe-Couloume, G., and Seyfried, W. E. (2007). Abiotic formation of hydrocarbons under hydrothermal conditions: constraints from chemical and isotope data. *Geochem. Cosmochim. Acta.* 71 (8), 1982–1998. doi:10.1016/j.gca.2007.01.022

Guélard, J., Beaumont, V., Rouchon, V., Guyot, F., Pillot, D., Jézéquel, D., et al. (2017). Natural H2in Kansas: deep or shallow origin?. *Geochem. Geophys. Geosyst.* 18 (5), 1841–1865. doi:10.1002/2016gc006544

Hawkes, H. E. (1972). Free hydrogen in genesis of petroleum: Geological notes. *AAPG Bull.* 56 (11), 2268–2270. doi:10.1306/819a4202-16c5-11d7-8645000102c1865d

Han, C. (2001). *Hydrocracking Process and Engineering (in Chinese)*. Beijing: China Petrochemical Press, 224–226.

He, K., Zhang, S., Mi, J., Chen, J., and Cheng, L. (2011). Mechanism of catalytic hydropyrolysis of sedimentary organic matter with MoS2. *Petrol. Sci.* 8 (02), 134–142. doi:10.1007/s12182-011-0126-0

Hirose, T., Kawagucci, S., and Suzuki, K. (2011). Mechanoradical H2 generation during simulated faulting: implications for an earthquake-driven subsurface biosphere. *Geophys. Res. Lett.* 38 (17), L17303. doi:10.1029/2011gl048850

Hosgörmez, H. (2007). Origin of the natural gas seep of Çirali (Chimera), Turkey: site of the first Olympic fire. *J. Asian Earth Sci.* 30 (1), 131–141. doi:10.1016/j.jseaes.2006.08.002

Jeffrey, A. W. A., and Kaplan, I. R. (1988). Hydrocarbons and inorganic gases in the gravberg-1 well, siljan ring, Sweden. *Chem. Geol.* 71 (1–3), 237–255. doi:10.1016/0009-2541(88)90118-0

Jia, W., Wang, Q., Liu, J., Peng, P., Li, B., and Lu, J. (2014). The effect of oil expulsion or retention on further thermal degradation of kerogen at the high maturity stage: a pyrolysis study of type II kerogen from Pingliang shale, China. *Org. Geochem.* 71, 17–29. doi:10.1016/j.orggeochem.2014.03.009

Jin, Z., Zhang, L., and Yang, L. (2002). Preliminary study on geochemical characteristics of fluids in deep sedimentary basins and Hydrocarbon Accumulation Effect. [J]. *Earth Sci.* 27 (6), 659–665. doi:10.3321/j.issn:1000-2383.2002.06.001

Jin, Z., Zhang, L., Yang, L., and Hu, W. (2004). A preliminary study of mantle-derived fluids and their effects on oil/gas generation in sedimentary basins. *J. Petrol. Sci. Eng.* 41 (1–3), 45–55. doi:10.1016/s0920-4105(03)00142-6

Jin, Z., Hu, W., and Zhang, L. (2007). *Deep fluid activity and hydrocarbon accumulation effect [M]*. Beijing: Science Press.

Johns, W. D. (1979). Clay mineral catalysis and petroleum generation. *Annu. Rev. Earth Planet Sci. C.* 7 (1), 183–198. doi:10.1146/annurev.ea.07.050179.001151

Kissin, Y. V. (1987). Catagenesis and composition of petroleum: origin of n-alkanes and isoalkanes in petroleum crudes. *Geochem. Cosmochim. Acta.* 51 (9), 2445–2457. doi:10.1016/0016-7037(87)90296-1

Klein, F., Grozeva, N. G., and Seewald, J. S. (2019). Abiotic methane synthesis and serpentinization in olivine-hosted fluid inclusions. *Proc. Natl. Acad. Sci. U.S.A.* 116 (36), 17666–17672. doi:10.1073/pnas.1907871116

Klein, F., Tarnas, J. D., and Bach, W. (2020). Abiotic sources of molecular hydrogen on Earth. *Elements* 16 (1), 19–24. doi:10.2138/gselements.16.1.19

Lewan, M. D., Winters, J. C., and McDonald, J. H. (1979). Generation of oil-like pyrolyzates from organic-rich shales. *Science* 203 (4383), 897–899. doi:10.1126/science.203.4383.897

Lewan, M. D. (1997). Experiments on the role of water in petroleum formation. *Geochem. Cosmochim. Acta.* 61 (17), 3691–3723. doi:10.1016/s0016-7037(97)00176-2

Li, S., Lin, S., and Guo, S. (2002). Effects of minerals on kerogen pyrolysis hydrocarbon generation. *J. Petrol. Univ. (Nat. Sci.)* 26 (1), 69–74. doi:10.3321/j.issn:1000-5870.2002.01.022

Liu, Q., Dai, J., Jin, Z., Li, J., Wu, X., Meng, Q., et al. (2016). Abnormal carbon and hydrogen isotopes of alkane gases from the Qingshen gas field, Songliao Basin,

China, suggesting abiogenic alkanes? *J. Asian Earth Sci.* 115, 285–297. doi:10.1016/j.jseaes.2015.10.005

Liu, Q., Zhu, D., Meng, Q., Liu, J., Wu, X., et al. (2018). The scientific connotation of oil and gas formations under deep fluids and organic-inorganic interaction[J]. *Science China Earth Sciences.* doi:10.1007/s11430-018-9281-2

Liu, J., Liu, Q., Zhu, D., et al. (2019). The function and impact of deep fluid on the organic matter during the hydrogeneration and evolution process[J]. *J. Nat. Gas Geosci.* 4 (4), doi:10.1016/j.jnggs.2019.07.002

Liu, J., and Tang, Y. (1998). Kinetics of early methane generation from Green River shale. *Chin. Sci. Bull.* 43 (22), 1908–1912. doi:10.1007/bf02883470

Liu, Q., Zhu, D., Meng, Q., Liu, J., Wu, X., Zhou, B., et al. (2018). Basic connotation of hydrocarbon Formation under deep fluid and Organic-inorganic interaction. *Sci. China Earth Sci.*, 1–22.

Lu, S., Xue, H., and Li, J. (2010). *Dynamics of isotope fractionation of natural gas and hydrocarbon and its application [M]*. Beijing: Petroleum Industry Press.

Luo, Y. (2004). *Handbook of chemical bond energy data*. Beijing: Science Press, 1–396.

Lv, Y., Liu, S., Wu, H., Hohl, S. V., Chen, S., Li, S., et al. (2018). Zn-Sr isotope records of the Ediacaran Doushantuo Formation in South China: diagenesis assessment and implications[J]. *Geochimica et Cosmochimica Acta*, 239, doi:10.1016/j.gca.2018.08.003

Ma, X., Zheng, G., Sajjad, W., Xu, W., Fan, Q., Zheng, J., et al. (2018). Influence of minerals and iron on natural gases generation during pyrolysis of type-III kerogen. *Mar. Pet. Geol.* 89, 216–224. doi:10.1016/j.marpetgeo.2017.01.012

Mango, F. D. (1996). Transition metal catalysis in the generation of petroleum and natural gas. *Geochem. Cosmochim. Acta.* 56 (1), 553–555. doi:10.1016/0016-7037(92)90153-a

Mango, F. D. (1996). Transition metal catalysis in the generation of natural gas. *Org. Geochem.* 24 (10–11), 977–984. doi:10.1016/s0146-6380(96)00092-7

Mango, F. D., and Hightower, J. (1997). The catalytic decomposition of petroleum into natural gas. *Geochem. Cosmochim. Acta.* 61 (24), 5347–5350. doi:10.1016/s0016-7037(97)00310-4

Mango, F. D., Hightower, J. W., and James, A. T. (1994). Role of transition-metal catalysis in the formation of natural gas. *Nature* 368 (6471), 536–538. doi:10.1038/368536a0

McCollom, T. M. (2013). Laboratory simulations of abiotic hydrocarbon Formation in earth's deep subsurface. *Rev. Mineral. Geochem.* 75 (1), 467–494. doi:10.2138/rmg.2013.75.15

McCollom, T. M. (2016). Abiotic methane formation during experimental serpentinization of olivine. *Proc. Natl. Acad. Sci. U.S.A.* 113 (49), 13965–13970. doi:10.1073/pnas.1611843113

Meng, Q., Sun, Y., Tong, J., Fu, Q., Zhu, J., Zhu, D., et al. (2015). Distribution and geochemical characteristics of hydrogen in natural gas from the Jiyang Depression, Eastern China. *J. Acta Geol. Sin. (Engl. Ed.)* 89 (5), 1616–1624. doi:10.1111/1755-6724.12568

Milesi, V., Mccollom, T. M., and Guyot,, F. (2016). Thermodynamic constraints on the formation of condensed carbon from serpentinization fluids [J]. *Geochimica Et Cosmochimica Acta.* 391–403. doi:10.1016/j.gca.2016.06.006

Newell, K. D., Doveton, J. H., Merriam, D. F., Lollar, B. S., Waggoner, W. M., and Magnuson, L. M. (2007). H2-rich and hydrocarbon gas recovered in a deep precambrian well in northeastern Kansas. *Nat. Resour. Res.* 16 (3), 277–292. doi:10.1007/s11053-007-9052-7

Pan, C., Yu, L., Liu, J., and Fu, J. (2006). Chemical and carbon isotopic fractionations of gaseous hydrocarbons during abiogenic oxidation. *Earth Planet Sci. Lett.* 246 (1–2), 70–89. doi:10.1016/j.epsl.2006.04.013

Pinto, F., Gulyurtlu, I., Lobo, L. S., and Cabrita, I. (1999). The effect of catalysts blending on coal hydropyrolysis. *Fuel* 78 (7), 761–768. doi:10.1016/s0016-2361(98)00212-9

Resing, J. A., Sedwick, P. N., German, C. R., Jenkins, W. J., Moffett, J. W., Sohat, B. M., et al. (2015). Basin-scale transport of hydrothermal dissolved metals across the South Pacific Ocean. *Nature* 523 (7559), 200–203. doi:10.1038/nature14577

Seewald, J. S. (2003). Organic-inorganic interactions in petroleum-producing sedimentary basins. *Nature* 426 (6964), 327–333. doi:10.1038/nature02132

Sherwood Lollar, B., Onstott, T. C., Lacrampe-Couloume, G., and Ballentine, C. J. (2014). The contribution of the Precambrian continental lithosphere to global H2 production. *Nature* 516 (7531), 379–382. doi:10.1038/nature14017

Shuai, Y., Zhang, S., Su, A., et al. (2010). Geochemical evidence for strong ongoing methanogenesis in Sanhu region of Qaidam Basin[J]. *Science in China*, 53 (001): 84–90. doi:10.1007/s11430-009-0081-4

Suda, K., Ueno, Y., Yoshizaki, M., Nakamura, H., Kurokawa, K., Nishiyama, E., et al. (2014). Origin of methane in serpentinite-hosted hydrothermal systems: the CH4-H2-H2O hydrogen isotope systematics of the Hakuba Happo hot spring. *Earth Planet Sci. Lett.* 386, 112–125. doi:10.1016/j.epsl.2013.11.001

Telling, J., Boyd, E. S., Bone, N., Jones, E. L., Tranter, M., MacFarlane, J. W., et al. (2015). Rock comminution as a source of hydrogen for subglacial ecosystems. *Nat. Geosci.* 8 (11), 851–855. doi:10.1038/ngeo2533

Thompson, R. R., and Creath, W. B. (1966). Low molecular weight hydrocarbons in Recent and fossil shells. *Geochem. Cosmochim. Acta.* 30 (11), 1137–1152. doi:10.1016/0016-7037(66)90034-2

Tivey, M. (2007). Generation of seafloor hydrothermal vent fluids and associated mineral deposits. *Oceanogr.* 20 (1), 50–65. doi:10.5670/oceanog.2007.80

Wu, L. M., Zhou, C. H., Keeling, J., Tong, D. S., and Yu, W. H. (2012). Towards an understanding of the role of clay minerals in crude oil formation, migration and accumulation. *Earth Sci. Rev.* 115 (4), 373–386. doi:10.1016/j.earscirev.2012.10.001